Chapter 9

Comparative Analysis of Conventional and Consequent-Pole External Rotor Brushless DC Motors for Electric Bicycle Applications

İbrahim Aydın[1]

Onur Özdal Mengi[2]

Serdal Arslan[3]

Abstract

The use of brushless direct current motors in electric/hybrid vehicles is increasing due to several advantages, such as the absence of rotor copper losses, high efficiency, smaller volume compared to motors of the same power, silent operation, and low maintenance requirements. In this study, the parameters of a surface-mounted permanent magnet brushless DC motor with an external rotor, designed for use in electric bicycles, were taken as a reference. Based on these parameters, an improved motor design with low cost and high output torque was aimed for. Different slot-to-pole ratio ranges were considered for each of the four different slot/pole models. To obtain performance data for the motors, ANSYS Maxwell is used for analyzing both the conventional model and the consequent pole model, respectively. Parameters such as cogging torque, power, and efficiency were calculated using ANSYS/Maxwell 3D software to obtain results that closely resemble application performance. The analysis shows improvements in torque, output power, total mass, and cost parameters for the consequent pole brushless DC motor compared to the conventional external rotor brushless DC motor with the same power and speed. In both models, the increase in operating temperature caused a decrease in engine performance data. However, while

1 High Engineer, Giresun Governorship Information Processing Branch Directorate, ibrahimaydin2806@gmail.com, ORCID: 0000-0002-1027-5230

2 Prof. Dr, Giresun University, Faculty of Engineering, Electrical and Electronics Engineering, onur.ozdal.mengi@giresun.edu.tr, ORCID: 0000-0001-5669-0766

3 Doç. Dr., Harran University, Organized Industrial Vocational Higher School, serdalarslan@harran.edu.tr, ORCID: 0000-0002-1187-5633

https://doi.org/10.58830/ozgur.pub776.c3235

there was no significant difference in terms of total motor mass between the models, the average efficiency of the conventional outer rotor BLDC motor was approximately 8,8% higher. Conversely, the consequent pole brushless DC motor was approximately 45% more affordable in terms of total cost. Thus, the 36-slot, 38-pole consequent pole outer rotor BLDC motor was determined to be more suitable than the different slot-pole combinations considered in this study. This design is expected to make a significant contribution to research on the cost-effective production of lightweight electric vehicles.

1. INTRODUCTION

Considering bicycles as a part of our daily life, it has a vital role in both health benefits and as a means of transportation. If the electric motor operates while the bicycle is moving with the mechanical energy created by the user in the pedal, there is no need for user-generated mechanical energy, and the bicycle has a hybrid structrure where mechanical and electrical energy are combined. With a hybrid model, the main structure of the bicycle is preserved, and additional equipment such as a battery, electric motor, and other components are added to transform it into an electric bicycle. This allows the bicycle to travel longer distances thanks to the motor powered by the battery.

Brushless direct current motors (BLDC) are commonly used in electric bicycle applications where these motors stand out in terms of driver hardware, controllability, maintenance, speed-torque characteristics, and efficiency. From this perspective, external rotor BLDC motor studies have been focused on electric bicycles.

Motor powers can range from 250 W to 750 W, and the speed limit can range from 20 km/h to 32.2 km/h [1]. According to the EN 15194 European standard, the electrical part of these pedal-assist electric bicycles is designed [2] . In our country, studies on electric bicycle motors should take into account the 250 W power and 25 km/h speed limit according to the Traffic Law No. 2918 [3].

Different concentrated winding structures are used in the stator structure of BLDC motors. In Ref. [4], on the effect of the slot/pole ratio of BLDC motors has been studied, and it has been shown that motors with slot/pole configurations of 36/34 and 36/38 exhibit the desired cogging torque, lightweight design, and high efficiency characteristics. The motor performances were very close to each other. It was also shown that the double-layer concentrated winding is more efficient than the single-layer concentrated winding, and the 36/34 slot motor achieves the same performance with fewer magnets than the open-slot motor. Although using open slots reduces the cost of stator winding production and allows it to be done more quickly, it has been shown that manufacturing costs and production speed increase due to difficulties in coil assembly in semi-closed slot structures. However, losses are less compared to open slot structures [5].

In a study comparing concentrated pole (CP) permanent magnet (CPPM) motors with different slot/pole numbers to traditional PM motors [6], it was shown that although both motors have the same output torque, the CPPM structure is 18.5% more efficient, and double-row harmonics causing large torque fluctuations can be eliminated with a new model in the 6/4 slot/pole CPPM motor.

In a simulation study on four different slot/pole combinations of outer rotor BLDC motor using ANSYS-Maxwell 3D software [7], it was shown that torque fluctuation was higher in the 36/16 slot/pole structure than the 24/16 slot/pole structure, and stator current density was higher than expected in the 48/22 and 72/32 slot/pole motors, indicating losses due to the high current density.

Finite element method (FEM) analyses were performed on evaluate the motor performance of various slot/pole models of outer rotor BLDC motors while ensuring that parameters such as power, voltage, rated speed, wheel diameter, permanent magnet, slot fill factor, etc., remained consistent. The effects of each motor model on copper and iron losses, as well as efficiency, were compared. As a result of this comparison, it has been shown that the efficiency of the model with a 24/20 slot/pole ratio is higher and the total loss is lower than the others [8].

As the volume of permanent magnets used in CPPM motors increases and the angular width of the used permanent magnets increases compared to traditional structures, the thickness of the permanent magnets required to achieve efficiency and nominal torque decreases. For this reason, if iron poles are used instead of permanent magnets in some of the poles of CPPM motors, the flux density distribution in the air gap can be improved, while the volume of the permanent magnet can be reduced when using the CP form compared to traditional methods [9].

In the study [10] on a new CPPM motor model with an image pole pair for each pole pair of N and S poles, it has been shown that the formation of image pole pairs in the iron core parts as well as the actual surface PM in the rotor allows the high-speed operating range to be expanded efficiently without increasing copper loss. However, it was emphasized that more research should be done on this model due to the low amount of effective magnetic flux and lower torque in the low speed range.

In a study [11] conducted on CPPM and Surface-Mounted Permanent Magnet (SMPM) rotor models, it has been demonstrated that the CPPM rotor model uses 50% less magnets compared to the SMPM rotor model. Although the magnetization property is weaker in the CPPM rotor model, it can be overcome with appropriate design and magnet material selection. In terms of cost, it has been shown that the CPPM rotor structure can be designed to be 13% more cost-effective compared to the SMPM rotor structure. The study [12] conducted on the simple yet powerful analytical modeling technique developed to calculate the radial force on the rotor of the CPPM engine has shown that it may be possible to calculate the force in various scenarios, such as rotor dynamic eccentricity, static eccentricity, or vibrations in the rotor air gap.

In a study [13] comparing the outer rotor traditional SMPM brushless motor with the CPPM brushless motor; it has been found that the CPPM motor has a maximum tooth torque 10 times greater than that of the SMPM motor. This is despite the fact that in the CPPM motor, half of the magnets have been removed, leading to a 50% reduction in magnet cost. However, the efficiency of the CPPM motor decreased by 3% compared to the SMPM motor although, it has been shown that even though the inductances in SMPM motors do not vary significantly with rotor position, the CPPM brushless motor has a changing inductance, resulting in the emergence of a new component of magnetic torque.

Parameters such as cost, efficiency, power, torque and cogging torque are very important for SMPM and CPPM in the engines of small or large power electric vehicles. The study is divided into five sections:

In the first section; previous analyses related to electric bicycle motors from theses and articles have been reviewed. This section serves as a literature review to provide background information on the subject. The second section; focusing on the sizing quantities of outer rotor BLDC, information about reference engine label information, sizing quantities and analysis materials is given. The third section; discusses the results obtained with Ansys Maxwell. It examines selected slot/pole combinations, winding structures, winding factors, torque, and torque ripple while aiming to achieve an appropriate design. The goal here is to propose the use of consequent-pole outer rotor BLDC as an alternative for electric bicycle applications, comparing it to traditional models. For this purpose, it has been suggested that the consequent-pole outer rotor BLDC can be used for electric bicycle applications compared to the traditional model. In the last section; conclusions regarding the findings that will support this suggestion are given.

2. BLDC MACHINE ANALYTICAL MODEL AND THEORETICAL CALCULATION

2.1 Basic Parameters of BLDC

The torque produced in an engine is calculated as in Equation 1:

$$T = \frac{1}{2} i^2 \frac{dL}{d\theta} - \frac{1}{2} \phi_g{}^2 \frac{dR}{d\theta} + Ni \frac{d\phi_g}{d\theta} \tag{1}$$

where, i is current passing through the coil (Ampere), L is coil inductance (H), θ is angular rotor position (°), R is reluctance of the magnetic circuit and $\emptyset_g$ is air gap flux (Weber).

The back electromotive force per phase in a permanent magnet motor is calculated as shown in Equation 2, and the air gap flux is calculated as shown in Equation 3.

$$E_0 = \frac{p}{2} \omega_m N_{tf} \phi_g k_w k_{st} \tag{2}$$

$$\phi_g = \overline{B_g} A_k \tag{3}$$

where, E_0 is back electromotive force (V), P is number of poles, ω_m is mechanical speed of the rotor (rad/s), N_{tf} is number of turns per phase, k_w is winding factor, k_{st} is stacking factor, B_g is air gap flux density (Wb/m²), and A_k is pole cross-sectional area (mm²).

The EMF constant k_e is given in Equation 4 as follows:

$$k_e = \sqrt{3} \frac{p}{2} N_{tf} B_g k_w k_{st} \tag{4}$$

The back electromotive force is given by Equation 5 over the mechanical speed and Equation 4:

$$E_0 = \omega_m k_e \tag{5}$$

The electromagnetic output power is shown in Equation 6, and the torque is represented in Equation 7 as follows:

$$P_e = 3E_0 I_q \tag{6}$$

$$T_e = \frac{3E_0 I_q}{\omega_m} \tag{7}$$

Using Equation 4, Equation 5 and Equation 7, the torque equation in Equation 8 is derived.

$$T_e = \sqrt{3}\frac{p}{2} N_{tf} \bar{B}_g k_w k_{st} I_q \tag{8}$$

Since torque is linear with I_q, the torque becomes as shown in Equation 9:

$$T_e = k_{st} I_q \tag{9}$$

2.2 Radial Force

In a good motor design, it is expected that the net radial force is low. The primary reason for the radial force in the motor is the interaction between the stator steel and the permanent magnets in the rotor. The value of t ($t=N_s/2p$), defined as the ratio of the number of stator slots (N_s) to the number of poles ($2p$), is an indicator of the radial force. If the t value is equal to 1 or an odd number, it indicates that the motor has a high net radial force, whereas if it is greater than 1 or an even number, it is a measure of the motor having a low net radial force. Therefore, the selected motor should have an even t value to minimize the net radial force [4].

2.3 Winding Factor

The winding factor k_{wn}, which is referred to as effective turns in phase windings, is expressed as shown in Equation 10 [14]:

$$k_{wn} = \frac{1}{N_{cph}} \sum_{k=1}^{N_{cph}} e^{-jn\theta_k} \tag{10}$$

where, N_{cph} is the number of slots per phase, n is harmonic index, and θ_k represents the relative angular displacement of coil number k [14].

The number of slots per phase is expressed as shown in Equation 11:

$$N_{cph} = \frac{N_s}{N_{ph}} = \frac{N_s}{3} \tag{11}$$

The electrical relative angle of all coils within slot number k is expressed as shown in Equation 12 [15]:

$$\theta_k(k) = (k-1)\frac{N_m}{N_s}180°E \tag{12}$$

2.4 Slot Fill Factor

The slot fill factor is a measure that indicates how much of the slots in an electric motor's stator are filled with coils. The slot fill factor is an important factor that affects the motor's design, efficiency, torque production, and heat generation. This ratio can vary depending on the motor winding structure (concentrated, distributed, etc.). Not only a higher slot fill factor can increase motor efficiency and torque production, but it also leads to the use of more materials and can complicate labor and production costs.

Selecting the slot fill factor correctly in motor design is essential. To design the motor, this ratio can be chosen between 40% and 65%. In this study, the slot fill factor has been chosen as 55%. Before calculating the slot fill factor, some data such as conductor diameter and conductor cross-sectional area need to be calculated, and the expressions related to this are shown below.

$$A_{wc} = \frac{\pi D_{wc}^{\;2}}{4} \tag{13}$$

where, D_{wc} is the conductor diameter (mm), and A_{wc} represents the conductor cross-sectional area (mm^2).

If there is not information about the conductor diameter in the software, the conductor cross-sectional area (A_{wc}) can be expressed as shown in Equation 14:

$$A_{wc} = \frac{A_s k_{wc}}{2N} \tag{14}$$

where, A_s is slot area (mm^2), k_{wc} is the slot fill factor, and N is the number of turns in a coil or winding.

The slot fill factor is expressed as shown in Equation 15 [16]:

$$k_{wc} = \frac{2NAk_{wc}}{2N} \tag{15}$$

2.5 Sizing study

In motor sizing studies, it is essential to know the desired torque or output power and speed for the motor. The sizing process typically begins with analytical calculations. Subsequently, various software tools (such as Ansys, MotorCad, Speed, etc.) are used to perform motor data calculations and analysis with the help of finite element analysis (FEA). In this study, an external rotor BLDC (Brushless DC) motor has been selected.

Figure 1-2 shows the common parameters of an internal rotor BLDC motor [17], while Figure 2 illustrates the stator and rotor parameters of an external rotor traditional BLDC motor, and Figure 3 displays the stator and rotor parameters of an external rotor segmented pole BLDC motor [18].

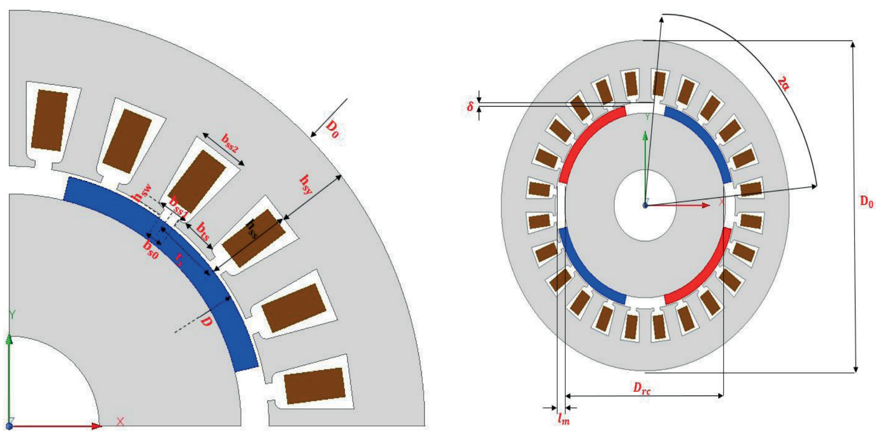

(a) *(b)*

Figure 1

(a) Representation of geometric parameters of stator and rotor in a quarter section of an inner rotor BLDC motor, and (b) Full view of the BLDC motor with inner and outer diameter parameters

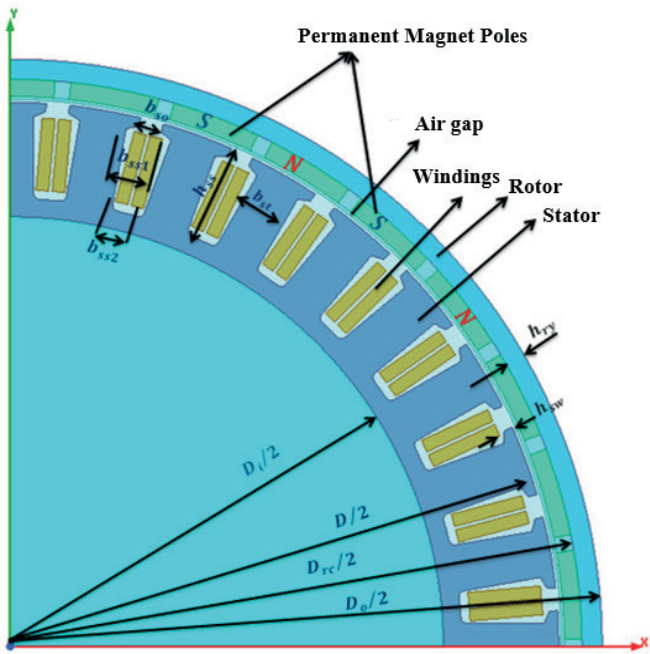

Figure 2 Representation of some geometric parameters for a 1/4 section of 36 slots and 34 poles the outer rotor traditional BLDC motor.

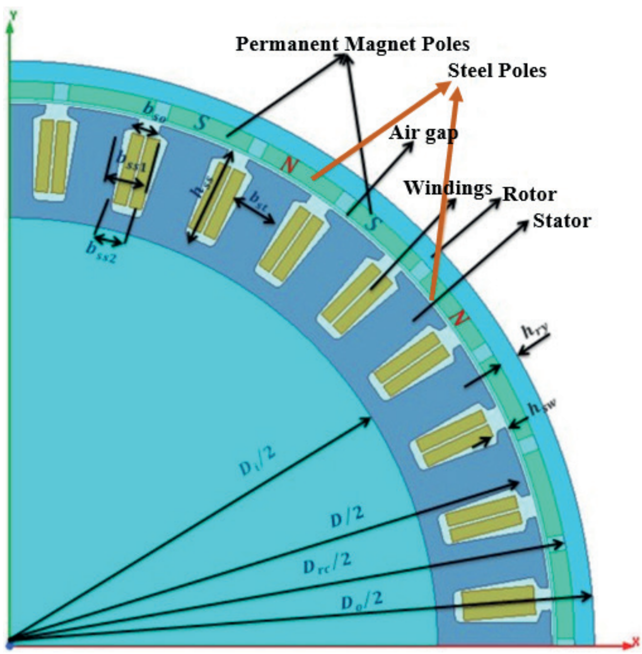

Figure 3 Representation of some geometric parameters for a 1/4 section of 36 slots and 34 poles the outer rotor consequent-pole BLDC motor.

In sizing studies, determining the stator and rotor diameter dimensions along with the motor length is of great importance. For an external rotor BLDC motor, find the stator's outer diameter using the equation in Equation 16:

$$D = D_{rc} - 2l_m - 2\delta \tag{16}$$

where, D is the stator's outer diameter, D_{rc} is the rotor's inner diameter, l_m is magnet thickness, and δ is the air gap length.

To achieve a uniform flux distribution in the stator and rotor cores as well as the air gap of a motor, it is necessary to design appropriate slots. In this context, Equation 17 provides the upper slot width value for the stator slot.

$$b_{ssl} = \pi \frac{D - 2h_{sw}}{N_s} - b_{st} \tag{17}$$

where, h_{sw} is stator tooth thickness, b_{ts} is the stator core tooth width, and N_s is number of stator slots.

Equation 18 provides the lower slot width value for the stator slot:

$$b_{ss2} = \pi \frac{D - 2h_{ss}}{N_s} - b_{st} \tag{18}$$

Equation 19 provides the effective core thickness value.

$$h_{sy} = \frac{1}{2}(D - D_i - 2h_{ss}) \tag{19}$$

where, h_{ss} is slot size, and D_i is stator's inner diameter. D_i is a parameter specific to an outer rotor BLDC motor only. Similarly, Equation 20 provides the thickness value of the core responsible for the flow of magnetic flux in the rotor.

$$h_{ry} = \frac{1}{2}(D_0 - D_{rc}) \tag{20}$$

where, h_{ry} is rotor's core thickness, representing the thickness of the core in the rotor. Equation 21 provides the total slot area on the stator.

$$A_{sl} = \frac{1}{2}(b_{ss1} + b_{ss2}) \times (h_{ss} + h_{sw}) \tag{21}$$

The ratio of the stator slot opening to the slot width is given in Equation 22:

$$k_{open} = \frac{b_{s0}}{b_{ss1}} \tag{22}$$

The parameters of the reference motor, which is a 250 W, 36-slot, 38-pole model designed for an electric bicycle, are shown in Table 1.

The slot characteristic are presented in Table 2, and the winding properties can be found in Table 3 [18].

Table 1 The fundamental and excitation circuit characteristics.

Parameters	**Values**	**Parameters**	**Values**
Motor Type	BLDC	Rated Voltage	48 V
Number of Slots	36	Number of phase (m)	3
Number of Poles	38	Circuit Type	Yıldız
Rotor Type	Outer Rotor	Control type	DC
Rated Speed	200 rpm	Magnet Thickness	3 mm
Motor Length	25 mm	Magnet Type	NdFeB35
Operating Temperature	75 ^{0}C	Embrace	0,84
Stator Inner Diameter	150 mm	Rotor Inner Diameter	192 mm
Stator Outer Diameter	190 mm	Rotor Outer Diameter	207 mm
Stator Steel Type	M19_26G	Stacking Factor	0,95

Table 2 Slot Design and Dimensions

Parameters	**Values**
Hs0	1,5 mm
Hs1	1 mm
Bs0	4 mm
Rs	1 mm

Table 3 The Stator Winding Properties

Parameters	**Values**
Winding Layers	2
Winding Type	Whole Coiled
Parallel Branches	1
Conductors per slot	25
Coil Pitch	1

3 NUMERICAL ANALYSİS RESULTS AND DISCUSSION

3.1 FEA with ANSYS-Maxwell 2D/3D

In the ANSYS Maxwell program, it is possible to obtain results closer to reality by conducting analyses initially performed in 2D in a three-dimensional (3D) manner [19]. However, 3D analyses depend on computer performance and can be time-consuming due to calculations based on electromagnetic equations through the 3D model structure. Therefore, 2D analysis is commonly used in various electric machine designs [19-23].

In this study, for the 3D analysis, the models were

first designed in three dimensions. Thereafter, consequent pole and conventional pole models are analyzed for the pole arc ratio with the smallest cogging torque. Parameters existing in 2D were recalculated using the inite Element Method (FEM) method. Subsequently, comparisons were made from various angles with the results of 2D analysis.

The 3D representation of the motor for the 36/38 slot/pole structure for both conventional and consequent pole structures are shown in Figure 4 (a) and (b), and the mesh representation on these models is depicted in Figure 5 (a) and (b) [24]. The mesh counts and analysis times for the models analyzed in 3D are shown in Table 4 below.

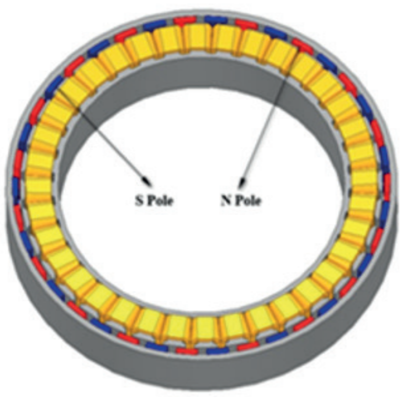

(a)

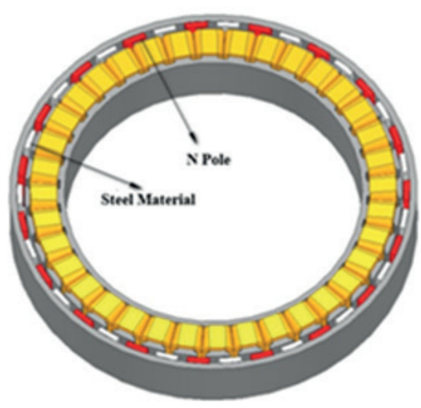

(b)

Figure 4 *(a) 3D representation of the conventional model, and (b) 3D representation of the consequent-pole model*

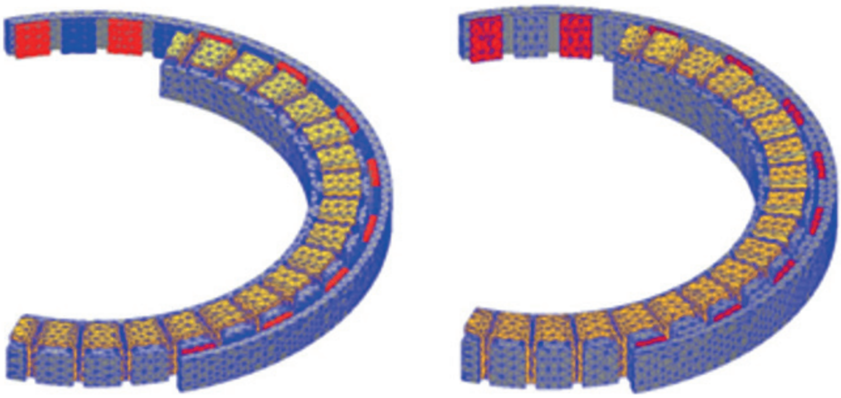
(a) (b)

Figure 5 *(a) Mesh representation of the conventional model, and (b) Mesh representation of the consequent-pole model*

Table 4 The mesh counts and analysis times for the conventional and consequent-pole models.

Pole Number	Pole Embrace	Model	2D/3D Analysis	Mesh (Number)	Analysis Time (minute)
34	0,8	NS	2D	4092	4 minute 10 second
	0,8		3D	100228	420 minute
	0,8	N	2D	4092	4 minute 18 second
	0,8		3D	95907	520 minute
38	0,75	NS	2D	4206	4 minute 11 second
	0,75		3D	99801	444 minute
	0,7	N	2D	4206	4 minute 26 second
	0,7		3D	100248	540 minute
40	0,8	NS	2D	1862	2 minute
	0,8		3D	50172	180 minute
	0,775	N	2D	1862	3 minute
	0,775		3D	50407	355 minute
42	0,8	NS	2D	1300	2 minute 41 second
	0,8		3D	33352	230 minute
	0,85	N	2D	1300	2 minute 44 second
	0,85		3D	33652	147 minute

**Where, NS is given as the traditional model, while N is given as the consequent pole.*

Table 4 reveals that as it break down the model into more elements to achieve results closer to reality, the analysis time tends to increase significantly. The data for the conducted analyses were obtained from a computer with an Intel i5 processor, 4 cores, and 8 GB of RAM. When using a more powerful hardware configuration, it is expected that the analysis process will be completed in a shorter time.

3.2 3D Analysis Results

For the four slot/pole configuration, the 3D analysis results for the embrace corresponding to the minimum cogging torque for conventional and consequent-pole models are shown in Table 5.

Table 5 3D analysis results for each pole structure.

Pole Number	Model	Analysis Type	Pole Embrace	Phase Current (A)	Ld (μH)	Lq (μH)	Pcore (W)	Pcu (W)	Torque (Nm)	Torque Increase/Decrease Ratio (%)	Pout (W)	Pout Increase/Decrease Ratio (%)	Efficiency (%)	Efficiency Increase/Decrease Ratio (%)
34	NS	3D	0,8	7,274	1.027,80	1.035,70	5,822	38,728	12,456	22,038	309,400	22,980	87,413	-9,433
	N	3D	0,8	11,328	1.336,600	1.395,000	6,192	93,931	15,201		380,499		79,168	
38	NS	3D	0,75	6,393	1.062,20	1.055,40	7,067	29,913	10,691	23,880	266,502	27,457	87,815	-10,178
	N	3D	0,7	10,811	1.340,700	1.374,000	5,402	85,561	13,244		339,676		78,877	
40	NS	3D	0,8	6,497	1.040,700	1.033,300	6,230	30,898	11,373	21,439	273,478	21,439	88,046	-6,661
	N	3D	0,775	9,546	1.359,000	1.409,000	5,304	66,704	13,811		332,110		82,181	
42	NS	3D	0,8	6,670	1.015,300	1.006,700	5,949	32,567	12,507	22,414	303,238	22,414	88,730	-7,510
	N	3D	0,85	10,149	1.321,000	1.337,000	5,720	75,398	15,310		371,207		82,066	

****Where, NS is given as the traditional model, while N is given as the consequent pole.***

In Table 5, it can be observed that in the results of the 3D analysis, traditional models have higher efficiency, while consequent-pole structures perform better in terms of output torque and output power.

In the 3D full-load analysis, the time-dependent variation of the output torque of 36 slot and 38 pole traditional and consequent-pole models are shown in Figure 6, and the change in a 3D phase current is shown in Figure 7.

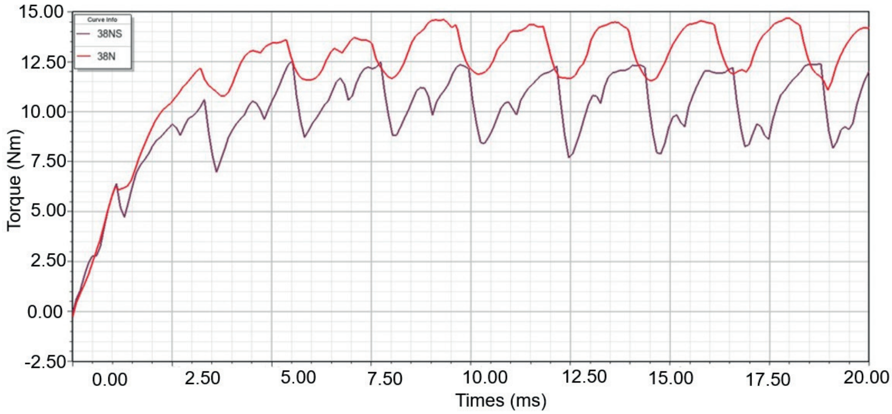

Figure 6 The change in output torque for both models in 3D

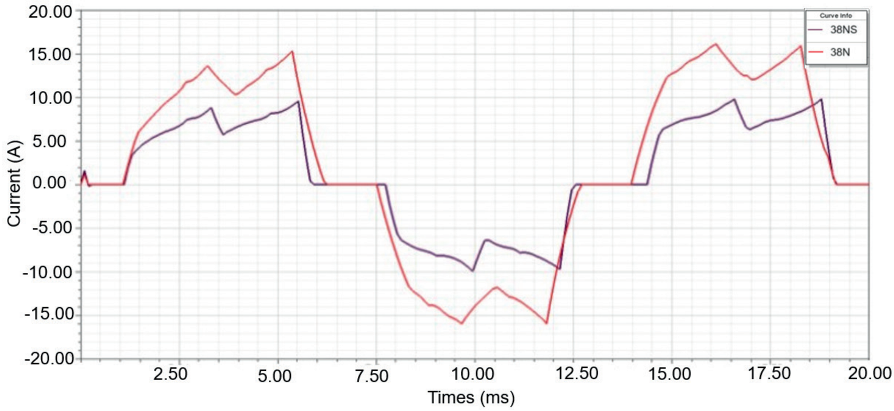

Figure 7 The change in phase current for both models in 3D

The difference between the calculations for 38-pole structure in RMxprt, 2D, and 3D is shown in Table 6.

Table 6 RMxprt, 2D, and 3D analysis results

Pole Number	Analysis Type	Model	Pole Embrace	Single Phase Current (A)	Single Phase Resistance	Pcore (W)	Pcu (W)	Rated Torque (Nm)	Rated Speed (Rpm)	Pin (W)	Pout (W)	Efficiency (%)
38	Rmxprt	NS	0,75	5,328	0,244	10,8348	15,483	9,41472	253,657	302,713	249,95547	82,5717676
	2D		0,75	4,4126	0,244	5,0101	14,2528	7,9497	253,657	230,32293	211,06002	91,6365684
	3D		0,75	6,3926	0,244	4,4146	29,9134	7,957	253,657	245,58186	211,25384	86,0217587

In Table 6, it can be observed that the phase current is 5,32 A in the RMxprt analysis, 4,41 A in the 2D analysis, and 6.39 A in the 3D analysis. The fact that the results in the 3D analysis are close to the results obtained in RMxprt indicates the proximity of the analytical values in the analysis conducted. Furthermore, it is expected that the values obtained by calculating the final winding inductance value in 3D will be different from the results obtained in 2D.The reason for this is the possibility to calculate the end winding inductance value in 3D. In Ref. [19], application results for the asynchronous motor have shown similar results to Rmxprt and Ansys Maxwell 2D. Additionally, even though the winding resistances are equal, the current magnitude affects copper losses, thus impacting efficiency.

Both the end winding inductance and the effects of non-linear behavior in steel materials, as well as leakage flux, are expected to cause variations in both motor output magnitudes in Rmxprt, Maxwell 2D, and 3D.

3.3 Comparison of 2D/3D Analysis Results for Models with Lower Cogging Torque.

In motor designs, while performing solutions in 2D analysis may provide convenience in terms of time, in order to trade-off the differences with more accurate comparison, all parameters obtained in 2D should also be calculated in 3D. Therefore, the 2D and 3D analysis results for these models are shown in Table 7.

Table 7 Comparison of 2D/3D Analysis Results

Pole Number	Model	Analysis Type	Pole Embrace	Phase Current (A)	Ld (μH)	Lq (μH)	Pcore (W)	Pcu (W)	Torque (Nm)	No Load Speed (rpm)	Pin (W)	Pout (W)	Efficiency (%)
34	NS	2D	0,8	6,842	847,915	855,699	4,491	34,269	12,157	237,327	304,715	343,430	88,727
		3D	0,8	7,274	1027,800	1035,700	5,822	38,728	12,456	237,327	309,400	353,950	87,413
	N	2D	0,8	10,869	1125,268	1177,704	3,906	86,490	15,429	237,327	383,270	473,666	80,916
		3D	0,8	11,328	1336,600	1395,000	6,192	93,931	15,201	237,327	380,499	480,623	79,168
38	NS	2D	0,75	7,042	865,307	865,199	4,560	36,299	12,875	229,994	309,943	350,802	88,353
		3D	0,75	6,393	1062,200	1055,400	7,067	29,913	10,691	229,994	257,361	294,341	87,436
	N	2D	0,7	11,584	1129,200	1167,400	4,014	98,220	15,985	229,994	384,812	487,045	79,009
		3D	0,7	10,811	1340,700	1374,000	5,402	85,561	13,244	229,994	318,819	409,782	77,802
40	NS	2D	0,8	6,509	851,426	850,572	4,773	31,023	11,961	229,741	287,627	323,422	88,932
		3D	0,8	6,497	1040,700	1033,300	6,230	30,898	11,373	229,741	273,478	310,606	88,046
	N	2D	0,775	10,817	1144,070	1204,757	4,308	85,670	15,154	229,741	364,392	454,371	80,197
		3D	0,775	9,546	1359,000	1409,000	5,304	66,704	13,811	229,741	332,110	404,117	82,181
42	NS	2D	0,8	6,452	832,647	832,486	4,847	30,480	11,700	231,650	283,686	319,012	88,926
		3D	0,8	6,670	1015,300	1006,700	5,949	32,567	12,507	231,650	303,238	341,754	88,730
	N	2D	0,85	10,712	1122,100	1143,700	4,256	83,807	15,288	231,650	370,681	458,743	80,803
		3D	0,85	10,149	1321,000	1337,000	5,720	75,398	15,310	231,650	371,207	452,324	82,066

3.4 Analysis of 36 slot 34 pole, 36 slot 38 pole, 36 slot 40 pole, and 36 slot 42 pole Models with in Terms of Cost

Untreated electrical silicon steel has been used as the stator and rotor steel. Arena Metal company was contacted for unit pricing, and the company provided a price per ton, which was used as the reference for unit cost [25].

N35 rare earth magnets have been used as permanent magnets. Since it was not possible to find a product with the exact volume and dimensions of the magnets used in our chosen model, the price could not be obtained. Therefore, for each known NdFeB magnet with known dimensions and price [26] on the Aliexpress website, the volume was calculated, and the mass in kilograms was determined by multiplying this volume by the density. With the known mass and price, the unit price of the magnets is calculated. The wire wound around the stator slots is enamel-coated copper wire, and the unit price of enamel wire with a conductor diameter of 0,50-1,00 mm is obtained from Emtel Enamel Wire company's website in Turkish Lira (TL) [27].It should be noted that, while getting the prices, the Turkish Lira/US Dollar exchange rate was 18,83.

The unit prices for the materials used in the selected model are shown in Table 8.

Table 8 The unit prices for the key materials used in BLDC.

Parameters	Material Unit Price (TL/kg)	Material Unit Price (USD/kg)
NdFeB Magnet	6651,37	358,18
Stator Winding	226,3	12,08
Stator and Rotor Steel	18,57	1

For these 4 models selected based on the cogging torque, there have been no changes in rotor and magnet dimensions, and winding turns. The total approximate cost price for each motor structure, i.e., motor body, cover, bearings, all labor, and VAT excluded, for both traditional and consequent pole structures are shown in Table 9. Additionally, Table 9 provides a comparison between the output torque, total weight, and efficiency obtained from the 3D analysis and the profit and loss ratio in total cost.

Table 9 The total cost prices for the model.

Pole Number	Model	PM Mass (kg)	Rotor Steel Mass (kg)	Stator Steel Mass (kg)	Stator Copper Mass (kg)	Motor Mass (kg)	The total cost of PM excluding VAT (T.L)	The total cost of Rotor and Stator Steel excluding VAT (T.L)	The total cost of Copper excluding VAT (T.L)	The total cost price excluding K.D.V (excluding labor))	The profit/loss percentage in total cost (excluding labor)
34	NS	0,324	0,451	1,384	0,507	2,665	2152,909	34,075	114,644	2300,970	46,65
	N	0,162	0,617	1,384	0,506	2,669	1076,454	37,159	114,508	1227,463	
38	NS	0,286	0,451	1,356	0,505	2,598	1899,625	33,548	114,384	2046,900	44,70
	N	0,148	0,598	1,356	0,505	2,607	981,875	36,289	114,386	1131,893	
40	NS	0,305	0,451	1,356	0,505	2,616	2026,267	33,544	114,381	2173,535	46,41
	N	0,153	0,603	1,356	0,505	2,617	1014,600	36,377	114,381	1164,701	
42	NS	0,314	0,451	1,352	0,505	2,623	2089,588	33,483	114,349	2236,763	43,53
	N	0,167	0,618	1,356	0,505	2,646	1112,822	36,651	114,381	1263,197	

****Where, NS is given as the traditional model, while N is given as the consequent pole.***

Table 10 Comparison of Models in Terms of Torque, Weight, Efficiency, and Total Cost.

Pole Number	Model	Output Torque (Nm)	Output Torque Increase/Decrease (%)	Efficiency (%)	Efficiency Increase/ Decrease (%)	Motor Mass (kg)	Total Engine Mass Increase/Decrease (%)	The total cost price excluding VAT (excluding labor)	The profit/loss percentage in total cost (excluding labor)
34	NS	12,456	22,04	89,473	-7,67	2,665	0,135	2300,970	46,65
	N	15,201		82,607		2,669		1227,463	
38	NS	10,691	23,88	89,130	-10,69	2,598	0,371	2046,900	44,70
	N	13,244		79,602		2,607		1131,893	
40	NS	11,373	21,44	89,880	-8,20	2,616	0,017	2173,535	46,41
	N	13,811		82,509		2,617		1164,701	
42	NS	12,507	22,41	89,811	-7,27	2,623	0,912	2236,763	43,53
	N	15,310		83,281		2,646		1263,197	

****Where, NS is given as the traditional model, while N is given as the consequent pole.***

The impact of reducing the number of permanent magnets by half when using a consequent pole rotor structure, where one pole pair has permanent magnets and the other pole pair is made of steel, on the motor cost can be evaluated considering the data provided in Table 10. It is evident that the chosen values for this motor are suitable for production. When considering mass production in a factory, a substantial cost reduction and increased profit margin become apparent.

3.5 The Impact of Temperature on Motor Parameters

In order to observe the impact of different operating temperatures on output values, a more temperature-resistant magnet material, specifically the N45UH magnet material from Arnold Magnetics, defined in the ANSYS Maxwell library with the B-H curve.

The choice of the pole structure for analysis was made based on the efficiency and output torque of the 4 models selected according to the impact moment, and a 42-pole structure was chosen. 3D analyses of this model were conducted at temperatures of 80°C, 120°C, and 150°C. The output values obtained from the analysis results are shown in Table 11. Additionally, the percentage changes in iron loss, torque, output power, and efficiency due to temperature variation are presented in Table 11.

Table 11 Output Parameters at Different Magnet Temperatures

Pole Number	Magnet Type	Model	Analysis Type	Pole Embrace	Operating Temperature, °C	Single Phase Current (A)	Single Phase Resistance (Ω)	Pcore (W)	Pcu(W)	Torque (Nm)	Rotor Speed (rpm)	Pout(W)	Efficiency (%)
42	N35UH	NS	3D	0,8	80	5,933	0,247	6,391	26,084	9,900	251,961	261,082	88,938
				0,8	120	5,839	0,278	6,071	28,434	9,275	260,782	253,163	88,005
				0,8	150	5,880	0,302	5,859	31,324	8,813	267,510	246,759	86,905
		N	3D	0,85	80	10,630	0,247	6,770	83,731	13,000	247,404	336,634	78,812
				0,85	120	10,410	0,278	5,667	90,379	12,030	256,072	322,430	77,049
				0,85	150	10,190	0,302	5,657	94,076	11,220	262,768	308,584	75,575

Where, NS is given as the traditional model, while N is given as the consequent pole.

The temperature causes the windings in the motor to heat up [28] and the magnetic flux strength of the magnets to decrease [29]. This situation affects the motor torque and efficiency [28-30]. At higher temperatures, irreversible demagnetization of magnets [29] and insulation problems in windings may occur [30]. Choi et al. [28] experimentally demonstrated the decrease in efficiency with increasing temperature in the BLDC motor. In Table 11, it can be observed that as magnet temperature increases, in both traditional and consequent pole structures, resistance and copper losses increase, while output torque, output power, and efficiency decrease.

Table 12 Percentage Change in Output Parameters Due to Temperature Variation

Model	Operating Temperature, °C	Pcore (W)	Torque (Nm)	Pout (W)	Efficiency (%)	Temperature Change		Pcore Increase/ Decrease Ratio(%)	Torque Increase/ Decrease Ratio (%)	Pout Increase/ Decrease Ratio (%)	Efficiency Increase/ Decrease Ratio (%)
NS	80	6,39	9,90	261,08	88,94	80 °C	120 °C	-5,00	-6,31	-3,03	-1,05
	120	6,07	9,28	253,16	88,01	120 °C	150°C	-3,51	-4,98	-2,53	-1,25
	150	5,86	8,81	246,76	86,90	80 °C	150 °C	-8,33	-10,98	-5,49	-2,29
N	80	6,77	13,00	336,63	78,81	80 °C	120 °C	-16,30	-7,46	-4,22	-2,24
	120	5,67	12,03	322,43	77,05	120 °C	150°C	-0,17	-6,73	-4,29	-1,91
	150	5,66	11,22	308,58	75,57	80 °C	150 °C	-16,44	-13,69	-8,33	-4,11

In Table 12, it can be observed that when the operating temperature is increased from 80°C to 120°C:

- In the traditional structure, there is an expected decrease of 5% in iron loss, 6,31% in output torque, 3% in output power, and 1,05% in efficiency.
- In the consequent -pole structure, there is an expected decrease of 16,30% in iron loss, 7,46% in output torque, 4,22% in output power, and 2,24% in efficiency.
- It proves that an increase in temperature results in greater changes in output parameters in the consequent pole structure. The most significant change is observed when the temperature is increased from 80°C to 150°C.

4. DISCUSSION AND CONCLUSIONS

In this study, parametric, 2D, and impact moment analyses were conducted for 4 different slot/pole models with varying winding numbers and pole arc ratios for both traditional and consequent pole structures. As a result of these analyses, models with the lowest impact moment were identified for both traditional and consequent pole structures. The identified models were subjected to 2D and 3D analyses as well as cost analyses. The analysis revealed that the 36-slot, 38-pole consequent pole outer rotor BLDC motor exhibited a low cogging torque and significantly high output torque and power. Furthermore, the effect of operating temperature on both traditional and consequent pole motors was evaluated.

Based on the results of the 3D analysis;

- The traditional outer rotor BLDC motor had an average efficiency that was approximately 8,8% higher.
- There was not a significant difference in total motor mass between the two models, except for the pole structure.
- The consequent pole outer rotor BLDC had approximately 16% higher output torque and power.
- Due to the reduction in the number of permanent magnets in the consequent pole outer rotor BLDC (excluding motor body, cover, bearings, all labor, and VAT), the total production cost was approximately 45% more favorable.
- An increase in operating temperature resulted in a decrease in motor performance data.
- It was previously shown in a different study that using a consequent pole outer rotor BLDC instead of an 8-pole, 9-slot surface-mounted structure reduced costs by around 50% and resulted in nearly a 3% decrease in efficiency [13]. In this study, with different slot/pole structures, it is observed that when compared to the traditional model, using an outer rotor consequent pole structure reduces costs by around 45%, supporting the findings of the previous study.

Considering the increasing costs of magnets, it becomes inevitable to implement motor designs with less magnet usage. From this perspective, the motor parameters used in the design, winding fill factor, and other aspects are suitable for manufacturing. The efficiency decrease observed in the consequent-pole structure can be improved through various optimization methods. Taking all these factors into account, it is believed that the recent interest in consequent-pole outer rotor BLDC motors will contribute to reducing production costs in various applications, especially in electric bicycles, and lead to the development of motors with competitive efficiency for their price segments.

5 References

[1] Hung, N. B., & Lim, O. (2020). A review of history, development, design and research of electric bicycles. Applied Energy, 260, 114323.

https://doi.org/10.1016/j.apenergy.2019.114323

[2] EN-15194. (2009). Cycles-Electrically power assisted cycles-EPAC Bicycles, European Committee For Standardization, Brussels. Retrieved from

https://cdn.standards.iteh.ai/samples/39396/68ab6cb984ae44c69626f7cdd050f238/SIST-EN-15194-2017.pdf

[3] Resmi Gazete (1983, October 18). 2918 Sayılı Karayolları Trafik Kanunu. Retrieved from https://www.mevzuat.gov.tr/mevzuat?MevzuatNo=8182&MevzuatTur=7&MevzuatTertip=5

[4] Tanç, G. (2014). Elektrikli bisikletler için fırçasız doğru akım motoru tasarımı ve üretimi (Doctoral dissertation, Fen Bilimleri Enstitüsü).

http://hdl.handle.net/11527/13192

[5] Lindh, P. M., Jussila, H. K., Niemela, M., Parviainen, A., & Pyrhonen, J. (2009). Comparison of concentrated winding permanent magnet motors with embedded and surface-mounted rotor magnets. *IEEE Transactions on Magnetics*, *45*(5), 2085-2089.

https://doi.org/10.1109/TMAG.2008.2011643

[6] Liu, D., Kan, G., & Mu, Y. (2020, November). Analysis of a consequent-pole permanent magnet machine for electric vehicle propulsion. In *2020 23rd International Conference on Electrical Machines and Systems (ICEMS)* (pp. 1615-1618). IEEE.

https://doi.org/10.23919/ICEMS50442.2020.9291005

[7] Dusane, P. M. (2016). Simulation of BLDC Hub Motor in ANSYS - Maxwell.

https://doi.org/10.13140/RG.2.1.2601.1764

[8] Çabuk, A. S., Sağlam, Ş., Tosun, G., & Üstün, Ö. (2016, December). Investigation of different slot-pole combinations of an in-wheel BLDC motor for light electric vehicle propulsion. In *2016 National Conference on Electrical, Electronics and Biomedical Engineering (ELECO)* (pp. 298-302). IEEE.

[9] Sakamoto, S., Yokoi, Y., Higuchi, T., & Miyamoto, Y. (2020, November). A study on rotor design of consequent-pole permanent magnet machines. In *2020 23rd International Conference on Electrical Machines and Systems (ICEMS)* (pp. 1600-1603). IEEE.

https://doi.org/10.23919/ICEMS50442.2020.9291128

[10] Noguchi, T., Murakami, K., Hattor, A., & Kaneko, Y. (2019, November). Proposal and operation characteristics of novel consequentpole perma-

nent magnet motor. In *Journal of Physics: Conference Series* (Vol. 1367, No. 1, p. 012032). IOP Publishing.

https://doi.org/10.1088/1742-6596/1367/1/012032

[11] Bai, J., Liu, J., Wang, M., Zheng, P., Liu, Y., Gao, H., & Xiao, L. (2018). Investigation of a less rare-earth permanent-magnet machine with the consequent pole rotor. *AIP Advances*, *8*(5).

https://doi.org/10.1063/1.5006861

[12] Dorrell, D. G., Amemiya, J., Chiba, A., & Takenaga, T. (2003, November). Analytical modelling of a consequent-pole bearingless permanent magnet motor. In *The Fifth International Conference on Power Electronics and Drive Systems, 2003. PEDS 2003.* (Vol. 1, pp. 247-252). IEEE.

https://doi.org/10.1109/PEDS.2003.1282776

[13] Ghaffari, A., Rahideh, A., Moayed-Jahromi, H., Vahaj, A., Mahmoudi, A., & Soong, W. L. (2019). 2-D analytical model for outer-rotor consequent-pole brushless PM machines. *IEEE Transactions on Energy Conversion*, *34*(4), 2226-2234.

https://doi.org/10.1109/TEC.2019.2941935

[14] Çağışlar, A., Tiryaki, H., & Bayhan, N. (2020). Effects of number of turns of armature winding on outer rotor brushless direct current motor designed for an electric vehicle prototype. *Niğde Ömer Halisdemir Üniversitesi Mühendislik Bilimleri Dergisi*, *9*(2), 832-847.

https://doi.org/10.28948/ngumuh.689396

[15] Hanselman, D. C.(2003). *Brushless permanent magnet motor design*. The Writers' Collective.

[16] Nory, H. (2018). Fırçasız doğru akım motorun tasarımı ve denetimi. *Elazığ Fırat University*.

[17] Aslan, N. (2020). *Elektrikli araçlar için fırçasız doğru akım motoru tasarımı* (Master's thesis, Fen Bilimleri Enstitüsü).

[18] Tuncel, E. (2019). *Elektrikli bisikletler için sabit mıknatıslı doğru akım motoru tasarımı ve optimizasyonu* (Master's thesis, Fen Bilimleri Enstitüsü).

[19] Arslan, S. (2016). Dalgıç Motorun Analitik, Sayısal, Performans Sonuçlarının Karşılaştırılması. Düzce Üniversitesi Bilim ve Teknoloji Dergisi, 4(2), 403-415.

[20] Mellah, H., Arslan, S., Sahraoui, H., & Hemsas, K. E. (2022). The effect of stator inter-turn short-circuit fault on dfig performance using fem. *Engineering, Technology & Applied Science Research*.

[21] Tarımer, İ., Arslan, S., & Güven, M. E. (2012). Investigation for losses of M19 and amorphous core materials asynchronous motor by finite elements methods. *Elektronika Ir Elektrotechnika*, *18*(9), 15-18. https://doi.org/10.5755/j01.eee.18.9.2797

[22] Balci, S., & Akkaya, M. (2022). Reduction of the core size and power losses by using soft magnetic material for a single-phase induction motor. *Measurement*, *198*, 111421.

https://doi.org/10.1016/j.measurement.2022.111421

[23] Özdil, A., & Uzun, Y. (2021). Design and analysis of a rotor for a 22 kW transversally laminated anisotropic synchronous reluctance motor.

https://doi.org/10.5755/j02.eie.29046

[24] ANSYS Electronics Suite 19.2.(2019).

[25] Tane Yönlendirilmemiş Silisli Sac.(2023, January 19). Retrieved from

http://www.arenametal.com.tr/celik/yassi-karbon-celik/silisli-sac/.

[26]Neodyum Mıknatıs Fiyatı.(2023, January 19). Retrieved from https://tr.aliexpress.com/w/wholesale-motor-neodyum magnets.html?catId=0&initiative_id=

SB_20221224055719&SearchText=motor%2Bneodyum%2Bmagnets&spm=a2g0o.home.1000002.0&dida=y.

[27] Emaye bobin fiyatı. (2023, January 19).Retrieved from https://shop.emtel.com.tr/emsold-180-hb-sinifi-emaye-bobin-teli-050-100.

[28] Choi, J., Lee, J. H., Jung, Y. G., & Park, H. (2020). Enhanced efficiency of the brushless direct current motor by introducing air flow for cooling. *Heat and Mass Transfer*, *56*, 1825-1831. https://doi.org/10.1007/s00231-020-02827-8

[29] Fernandez, D., Hyun, D., Park, Y., Reigosa, D. D., Lee, S. B., Lee, D. M., & Briz, F. (2017). Permanent magnet temperature estimation in PM synchronous motors using low-cost hall effect sensors. *IEEE Transactions on Industry Applications*, *53*(5), 4515-4525. https://doi.org/10.1109/TIA.2017.2705580

[30] Kuria, J., & Hwang, P. (2012). Investigation of thermal performance of electric vehicle BLDC motor. *International journal of mechanical engineering*, *1*(1), 1-17.